Publ. Astron. Soc. Japan (2021) 73 (1), 1–13
doi: 10.1093/pasj/psaa089
Advance Access Publication Date: 2020 October 2

Multi-wavelength photometry during the 2018 superoutburst of the WZ Sge-type dwarf nova EG Cancri

Mariko Kimura,[1,2,*] Keisuke Isogai,[1,3] Taichi Kato,[1] Naoto Kojiguchi,[1] Yasuyuki Wakamatsu,[1] Ryuhei Ohnishi,[1] Yuki Sugiura,[4] Hanami Matsumoto,[4] Sho Sumiya,[4] Daiki Ito,[4] Kengo Nikai,[4] Katsura Matsumoto,[4] Sergey Yu. Shugarov,[5,6] Natalia Katysheva,[5] Hiroshi Itoh,[7] Pavol A. Dubovsky,[8] Igor Kudzej,[8] Hiroshi Akitaya,[9,10] Kohei Oide,[11] Takahiro Kanai,[11] Chihiro Ishioka,[11] Yoshinori Uzawa,[12] Yumiko Oasa,[9,11,12] Tonny Vanmunster,[13] Arto Oksanen,[14] Tamás Tordai,[15] Katsuhiro L. Murata,[16] Kazuki Shiraishi,[16] Ryo Adachi,[16] Motoki Oeda,[16] Yutaro Tachibana,[16] Seiichiro Kiyota,[17] Elena P. Pavlenko,[18] Kirill Antonyuk,[18] Oksana Antonyuk,[18] Nikolai Pit,[18] Aleksei Sosnovskij,[18] Julia Babina,[18] Alex Baklanov,[18] Koji S. Kawabata,[10] Miho Kawabata,[10] Tatsuya Nakaoka,[10] Masayuki Yamanaka,[10] Kiyoshi Kasai,[19] Ian Miller,[20,†] Stephen M. Brincat,[21] Wei Liu,[22] Mahito Sasada,[10] and Daisaku Nogami[1]

[1]Department of Astronomy, Graduate School of Science, Kyoto University, Oiwakecho, Kitashirakawa, Sakyo-ku, Kyoto, Kyoto 606-8502, Japan
[2]Extreme Natural Phenomena RIKEN Hakubi Research Team, Cluster for Pioneering Research, RIKEN, 2-1 Hirosawa, Wako, Saitama 351-0198, Japan
[3]Okayama Observatory, Kyoto University, 3037-5 Honjo, Kamogatacho, Asakuchi, Okayama 719-0232, Japan
[4]Osaka Kyoiku University, 4-698-1 Asahigaoka, Kashiwara, Osaka 582-8582, Japan
[5]Sternberg Astronomical Institute, Lomonosov Moscow State University, Universitetsky Ave., 13, Moscow 119992, Russia
[6]Astronomical Institute of the Slovak Academy of Sciences, 05960 Tatranska Lomnica, Slovakia
[7]Variable Star Observers League in Japan (VSOLJ), 1001-105 Nishiterakata, Hachioji, Tokyo 192-0153, Japan
[8]Vihorlat Observatory, Mierova 4, Humenne, Slovakia
[9]Graduate School of Science and Engineering, Saitama University, 255 Shimo-Okubo, Sakura-ku, Saitama, Saitama 338-8570, Japan
[10]Hiroshima Astrophysical Science Center, Hiroshima University, 1-3-1 Kagamiyama, Higashi-Hiroshima, Hiroshima 739-8526, Japan
[11]Graduate School of Education, Saitama University, 255 Shimo-Okubo, Sakura-ku, Saitama, Saitama 338-8570, Japan
[12]Faculty of Education, Saitama University, 255 Shimo-Okubo, Sakura-ku, Saitama, Saitama 338-8570, Japan
[13]Center for Backyard Astrophysics (Belgium), Walhostraat 1A, B-3401, Landen, Belgium
[14]Hankasalmi Observatory, Jyvaskylan Sirius ry, Verkkoniementie 30, FI-40950 Muurame, Finland

[15]Polaris Observatory, Hungarian Astronomical Association, Laborc utca 2/c, 1037 Budapest, Hungary
[16]Department of Physics, Tokyo Institute of Technology, 2-12-1 Ookayama, Meguro-ku, Tokyo 152-8551, Japan
[17]VSOLJ, 7-1 Kitahatsutomi, Kamagaya, Chiba 273-0126
[18]Federal State Budget Scientific Institution "Crimean Astrophysical Observatory of RAS", Nauchny, 298409, Republic of Crimea
[19]Baselstrasse 133D, CH-4132 Muttenz, Switzerland
[20]Furzehill House, Ilston, Swansea, SA2 7LE, UK
[21]Flarestar Observatory, San Gwann SGN 3160, Malta
[22]Purple Mountain Observatory, Chinese Academy of Sciences, No.10 Yuanhua Road, Qixia District, Nanjing, 210023, China

*E-mail: mkimura@kusastro.kyoto-u.ac.jp
†Deceased 2020 June 12.

Received 2020 June 1; Accepted 2020 August 26

Abstract

We report on the multi-wavelength photometry of the 2018 superoutburst in EG Cnc. We have detected stage A superhumps and long-lasting late-stage superhumps via the optical photometry and have constrained the binary mass ratio and its possible range. The median value of the mass ratio is 0.048 and the upper limit is 0.057, which still implies that EG Cnc is one of the possible candidates for period bouncers. This object also showed multiple rebrightenings in this superoutburst which are the same as those in its previous superoutburst in 1996–1997, despite the difference in the main superoutburst. This would represent that the rebrightening type is inherent to each object and is independent of the initial disk mass at the beginning of superoutbursts. We also found that $B - I$ and $J - K_s$ colors were unusually red just before the rebrightening phase and became bluer during the quiescence between rebrightenings, which would mean that the low-temperature mass reservoir at the outermost disk accreted with time after the main superoutburst. Also, the ultraviolet flux was sensitive to rebrightenings as well as the optical flux, and the $U - B$ color became redder during the rebrightening phase, which would indicate that the inner disk became cooler when this object repeated rebrightenings. Our results thus basically support the idea that the cool mass reservoir in the outermost disk is responsible for rebrightenings.

Key words: accretion, accretion disks — novae, cataclysmic variables — stars: dwarf novae — stars: individual (EG Cancri)

1 Introduction

Cataclysmic variables (CVs) are close binary systems consisting of a white dwarf (the primary star) and a low-mass star (the secondary star). An accretion disk is formed around the primary via Roche-lobe overflow from the secondary. Dwarf novae (DNe) are a subclass of CVs and show outbursts representing a sudden release of gravitational energy. The mass accumulated at the disk in the quiescent state accretes on to the primary in the outburst state and a huge amount of gravitational energy is released during a short duration. This sudden accretion is triggered by the thermal-viscous instability in the disk [see Warner (1995) and Osaki (1996) for comprehensive reviews].

SU UMa-type stars, one of the subclasses of DNe, have short orbital periods ($\sim$1 hr $< P_{\rm orb} <$ $\sim$2 hr) and show occasional superoutbursts which are defined as large-amplitude ($\sim$6–8 mag) outbursts with superhumps. The superhumps are small-amplitude periodic light variations with periods slightly longer than the orbital period and are believed to be induced by the 3 : 1 resonance tidal instability (Whitehurst 1988; Osaki 1989; Hirose & Osaki 1990; Lubow 1991a, 1991b). Kato et al. (2009) investigated the time evolution of superhumps and proved that the superhumps have three stages: stage A superhumps with a long and constant period and increasing amplitudes, stage B superhumps with a systematically varying period and decreasing amplitudes, and stage C superhumps with a short and constant period.

WZ Sge-type stars, a subclass of SU UMa-type stars, have extremely small binary mass ratios and predominantly show superoutbursts. Here the mass ratio is defined as the ratio of the secondary mass with respect to the primary mass ($q \equiv M_2/M_1$). Double-peaked modulations, called "early superhumps", and rebrightening are their two representative observational properties (see Kato 2015 and references therein). Early superhumps have a period almost equal to the orbital one and are observed at the early stage of superoutbursts (Kato 2002; Ishioka et al. 2002). They are considered to be triggered by the 2 : 1 resonance tidal instability (Osaki & Meyer 2002, 2003). Rebrightening is usually observed soon after the main superoutburst with a long plateau stage and is classified into five types according to the morphology of light curves: type-A (long duration rebrightening), type-B (multiple rebrightenings), type-C (single rebrightening), type-D (no rebrightening), and type-E (double plateaus) (Imada et al. 2006; Kato et al. 2009, 2014a).

Rebrightenings in WZ Sge stars are not yet explained well by the current model of the disk instability. Some people argued that the mass transfer from the secondary star is temporally enhanced via the irradiation by the hot accretion disk (Hameury 2000; Patterson et al. 2002). However, it would be difficult for the irradiation to raise the mass transfer rate (Osaki & Meyer 2004), and no observational evidence of the increase of the mass-transfer rate has been detected. On the other hand, there is a possibility that substantial mass remains outside the 3 : 1 resonance radius, which accretes on the white dwarf delayed against the main superoutburst (Kato et al. 1998; Hellier 2001). A large amount of mass seems to be accumulated in the disk before superoutbursts because of long quiescence in WZ Sge stars, and once a superoutburst is triggered, the disk rapidly expands due to the angular-momentum transfer in the disk. Then the substantial mass is possibly conveyed beyond the 3 : 1 resonance radius (Osaki et al. 2001). The observational features like the presence of superhumps, the strong NaD absorption, the unusually red color, and the infrared activities, which were confirmed after the main superoutburst in some WZ Sge stars may support this idea (T. Kato et al. 1997;[1] Patterson et al. 1998; Uemura et al. 2008; Nakata et al. 2014; Isogai et al. 2015; Neustroev et al. 2017). Moreover, TCP J21040470+4631129, a recently observed WZ Sge-type star, triggered superoutbursts twice as a part of multiple rebrightenings after the main superoutburst (Tampo et al. 2020). This implies that there was a large mass reservoir in the outermost part of the disk and that any enhancement of mass transfer rates from the secondary star, which makes the disk shrink at the onset of rebrightenings, would not occur.

WZ Sge stars are interesting targets also in the study of the CV evolution because some of them are believed to be the best candidates for period bouncers. Period bouncers are defined as the post-period-minimum CVs containing degenerate secondaries. CVs evolve as the orbital period becomes shorter for a long time due to angular momentum losses by magnetic breaking and gravitational-wave radiation. Once the secondary star becomes degenerate, the system evolves as the orbital period becomes longer, since the thermal timescale of the secondary becomes longer than the mass-transfer timescale (see Knigge et al. 2011 and references therein). Although the population of period bouncers is predicted to be $\sim$70% of CVs by theoretical works, the number of the good candidates identified by observations is only around a few dozen (e.g., Kolb 1993; Littlefair et al. 2008; Nakata et al. 2014). The gap between observational and theoretical populations of period bouncers is one of the big problems in the CV evolution.

Kato and Osaki (2013) proposed a new dynamical method for estimating the binary mass ratio by using the period of stage A superhumps. The new method was applied to many WZ Sge-type stars, resulting in the identification of some period-bouncer candidates. Recent observations found that some of WZ Sge-type stars with type-B or type-E rebrightening are good candidates for period bouncers and that the candidates share the following common observational features: (1) repeating rebrightenings or dips in brightness at the main superoutburst stage, (2) long-lasting stage A superhumps, (3) large decreases in the superhump period at the stage A to B transition in the objects with repeating rebrightenings, (4) small superhump amplitudes ($\lesssim$0.1 mag), (5) long delays of the appearance of ordinary superhumps, (6) slow fading rates at the plateau stage with ordinary superhumps in the superoutburst, and (7) large outburst amplitudes at the time of appearance of ordinary superhumps (e.g., Nakata et al. 2014 and Kimura et al. 2018).

In this paper, we report on our multi-wavelength photometric observations of the 2018 superoutburst of the famous WZ Sge-type star EG Cnc which was originally discovered by Huruhata (1983). This system underwent a superoutburst in 1996–1997 (Patterson et al. 1998) and is supposed to have entered a normal outburst in 2009 (Templeton 2009). We started a photometric campaign of the 2018 superoutburst of this system soon after the detection of the luminosity increase by Patrick Schmeer. The mass ratio of EG Cnc was estimated to be 0.027–0.035 by using the superhump period in its 1996–1997 superoutburst, which is the smallest among the identified WZ Sge stars

[1] Kato, T., Nogami, D., Matsumoto, K., & Baba, H. 1997, preprint ⟨ftp://vsnet.kusastro.kyoto-u.ac.jp/pub/vsnet/preprints/EG_Cnc/⟩.

(Patterson et al. 1998; Patterson 2011), and hence, EG Cnc is considered to be the best candidate for period bouncers. However, the estimate was derived from the empirical relation between the excess of superhumps and the mass ratio (Patterson et al. 2005). Also, EG Cnc showed six consecutive rebrightenings just after the main superoutburst in the past. Each rebrightening is similar to a normal outburst with an interval of about a week, and hence, this target is suitable for the detailed observations of rebrightenings. Our purpose in this paper is to estimate more accurately the mass ratio of EG Cnc to examine if it is a possible period-bouncer candidate or not and to constrain the origin of multiple rebrightenings. This paper is structured as follows. We describe the methods of our observations and data analyses in section 2 and present the results in section 3. In section 4, we discuss the results, and a summary and conclusions are given in section 5.

2 Observations and analyses

Time-resolved optical and near-infrared (NIR) CCD photometry was carried out by the Variable Star Network (VSNET) collaboration team and the Optical and Infrared Synergistic Telescopes for Education and Research (Oister) at 21 sites. Table E1 shows the log of photometric observations.[2] All of the observation times are converted to barycentric Julian date (BJD). Each observer performed differential photometry. We have applied zero-point corrections to each observer by adding constants before analyses. The constancy of the comparison star that each observer used was checked by nearby stars within the same images. The observational log is summarized in table E1 in the supplementary information.[2]

The X-ray and ultraviolet (UV) observations were performed by the Swift/X-ray Telescope (XRT) and Swift/UltraViolet and the Optical Telescope (UVOT), respectively. The ObsIDs are 00035446003–00035446042. The X-ray data are processed through xrtpipeline. The UV flux is obtained via the standard tool uvot2pha provided by the Swift team. All of the observation times are converted to BJD as for the optical and NIR data.

We adopt the phase dispersion minimization (PDM) method (Stellingwerf 1978) for period analyses. Before applying PDM, we subtract the long-term trend of the light curve by locally weighted polynomial regression (LOWESS: Cleveland 1979). The 1σ error of the best-estimated period is determined by the same method as that described by Fernie (1989) and Kato et al. (2010). A variety of bootstraps was used for evaluating the robustness of the PDM result. We make 100 samples which randomly contained 50% of observations, and perform PDM analyses for these samples. The result of the bootstraps is expressed as a form of 90% confidence intervals in the resultant θ statistics. Also, we determine the times of maxima of ordinary superhumps in the same way as in Kato et al. (2009), when drawing the $O - C$ curve.

[2] Tables E1– E2 are available in the supplementary data section of the online version.

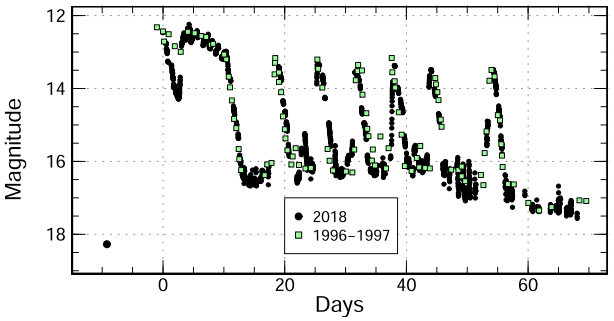

Fig. 1. Overall light curve of the 2018 superoutburst of EG Cnc (filled circles) compared with that in its 1996–1997 superoutburst (open rectangles). Day 0 of the 2018 superoutburst is adjusted to BJD 2458396.9184, and that of the 1996–1997 superoutburst is adjusted to BJD 2450420.1529, respectively. (Color online)

3 Results

3.1 Overall light curves

We show the overall light curve of the 2018 superoutburst of EG Cnc in figure 1 with the V-band light curve of its 1996–1997 superoutburst for comparison, which is derived from figure 1 of Patterson et al. (1998). Although it is unclear when the 2018 superoutburst began, the luminosity increase would occur at least after BJD 2458387.7. After the increase, the luminosity suddenly dropped by $\sim$2 mag around BJD 2458399 at the plateau stage. After the dip, the plateau continued during a week. Multiple rebrightenings (type-B rebrightening) were confirmed soon after the main superoutburst. The rebrightening behavior including the timing of each outburst in the 2018 superoutburst seems to be completely the same as that in the previous superoutburst. However, the depth of the luminosity dip in the plateau stage is different between these two outbursts. The duration of the plateau stage might be different as well.

3.2 Time evolution of superhumps

We have combined our R-band, V-band, and unfiltered data, and have made the $O - C$ curve of times of superhump maxima to search for superhumps. The $O - C$ curve before the rebrightening stage is given in the top panel of figure 2, with the amplitude of superhumps and the light curve in the middle and bottom panels. The $O - C$ value is summarized in table E2 in the supplementary information. Some points with large errors are removed from this

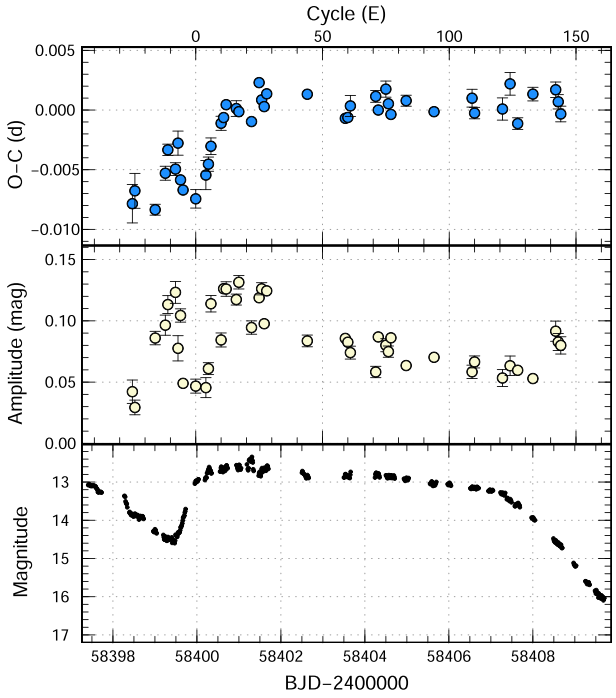

Fig. 2. Upper: $O - C$ curve of times of maxima of light modulations during BJD 2458398.4–2458408.7. An ephemeris of BJD 2458399.97+0.06032015 E is used for drawing this figure. Middle: Amplitude of humps. Lower: Light curve. The horizontal axis in units of BJD and the cycle number is common to these three panels. (Color online)

figure. According to the past studies on some WZ Sge stars entering superoutbursts with a luminosity dip in the middle of the plateau, there is a possibility that EG Cnc exhibited early superhumps before the dip (Kimura et al. 2018); however, we do not find them. It is unknown whether the lack of detection of early superhumps is attributed to the lack of observations or the fact that early superhumps did not develop.

Small-amplitude light variations seem to have appeared on BJD 2458398 and the onset of superhumps would be delayed with respect to the first appearance of the small-amplitude variations. The linear trend starting from the cycle 0 in the $O - C$ curve and the increasing amplitude of humps suggest that superhumps began developing on the cycle 0 and that the interval during BJD 2458399.7–2458400.8 ($0 \leq E \leq 12$) is stage A. The $O - C$ curve bends around the cycle 12, which means that the superhump period suddenly decreased. This indicates the onset of stage B superhumps. The period variation after this (see the texts in the next paragraph) and the decreasing amplitude of humps suggest that the interval during BJD 2458400.8–2458408.7 ($16 \leq E \leq 144$) is stage B. However, the fluctuations in the $O - C$ curve before the cycle 0 is not consistent with the observational properties of superhumps and early superhumps, which have been well investigated (see, e.g., Kato et al. 2009; Kato 2015).

The PDM results and the phase-averaged profiles of stage A superhumps, stage B superhumps, and light modulations before stage A are displayed in the upper left-hand, upper middle, and upper right-hand panels of figure 3. These modulations are clearly single-peaked. The stage A superhump period ($P_{\rm shA}$) estimated by PDM is 0.06103(2) d (see the upper left-hand panel of figure 3), and the averaged period at stage B ($P_{\rm shB}$) estimated by PDM is 0.060324(3) d, respectively (see the upper middle panel of figure 3). The derivative of the superhump period during stage B [$P_{\rm dot}(\equiv \dot{P}_{\rm sh}/P_{\rm sh})$] is $-1.5(4.0) \times 10^{-6}$ s s^{-1}. The averaged superhump amplitude during the plateau stage is 0.08 mag. On the other hand, the humps before the onset of stage A superhumps have a ∼0.0604-d period, which is shorter than the stage A superhump period and longer than the orbital period 0.05997(9) d (Patterson et al. 1998) (see the upper right-hand panel of figure 3). They do not seem to be either superhumps or early superhumps from their periodicity.

The superhumps seem to have continued for a long time after the main superoutburst. Long-lasting superhumps have been observed previously in WZ Sge stars, including EG Cnc itself (Patterson et al. 1998, 2002; Kato et al. 2008; Neustroev et al. 2017; Tampo et al. 2020). Figure 4 shows the $O - C$ curve of times of superhump maxima extending to the cycle ∼1200. Long-lasting late-stage superhumps seem to have begun at the cycle 215 in the 2018 superoutburst of EG Cnc. The superhumps in the cycles 181–200 may be of the end of stage C. As seen in some other WZ Sge-type superoutbursts, a ∼0.5 phase shift in superhumps seem to have occurred when this system entered the post-stage of the main superoutburst (see also Kato 2015) and this phenomenon was also confirmed in the 1996–1997 superoutburst of this object (Kato et al. 2004). This evolution of late-stage superhumps in the $O - C$ curve would be similar to that in the 1996–1997 superoutburst in EG Cnc (see also Patterson et al. 1998). Both of the $O - C$ curves seem to bend smoothly around the cycle 600. We can see that the superhump period fluctuated in the middle of the late-stage and that the period became constant again after that. We thus divide the late-stage superhumps into three intervals according to their period variations: during BJD 2458412.9–2458431.7 ($215 \leq E \leq 526$) as stage La, during BJD 2458435.5–2458453.7 ($590 \leq E \leq 891$) as stage Lb, and during BJD 2458457.5–2458471.7 ($956 \leq E \leq 1189$) as stage Lc. It is difficult to distinguish stage Lb and stage Lc, and we determine the time interval of stage Lc to minimize $P_{\rm dot}$. We give the PDM results and the phase-averaged profiles of stage La, stage Lb, and stage Lc superhumps in the lower left-hand, lower middle, and lower right-hand panels of figure 3. The superhump periods during stage La and stage Lc are 0.06050(1) d and 0.06042(2) d, respectively. The averaged superhump period in stage Lb is

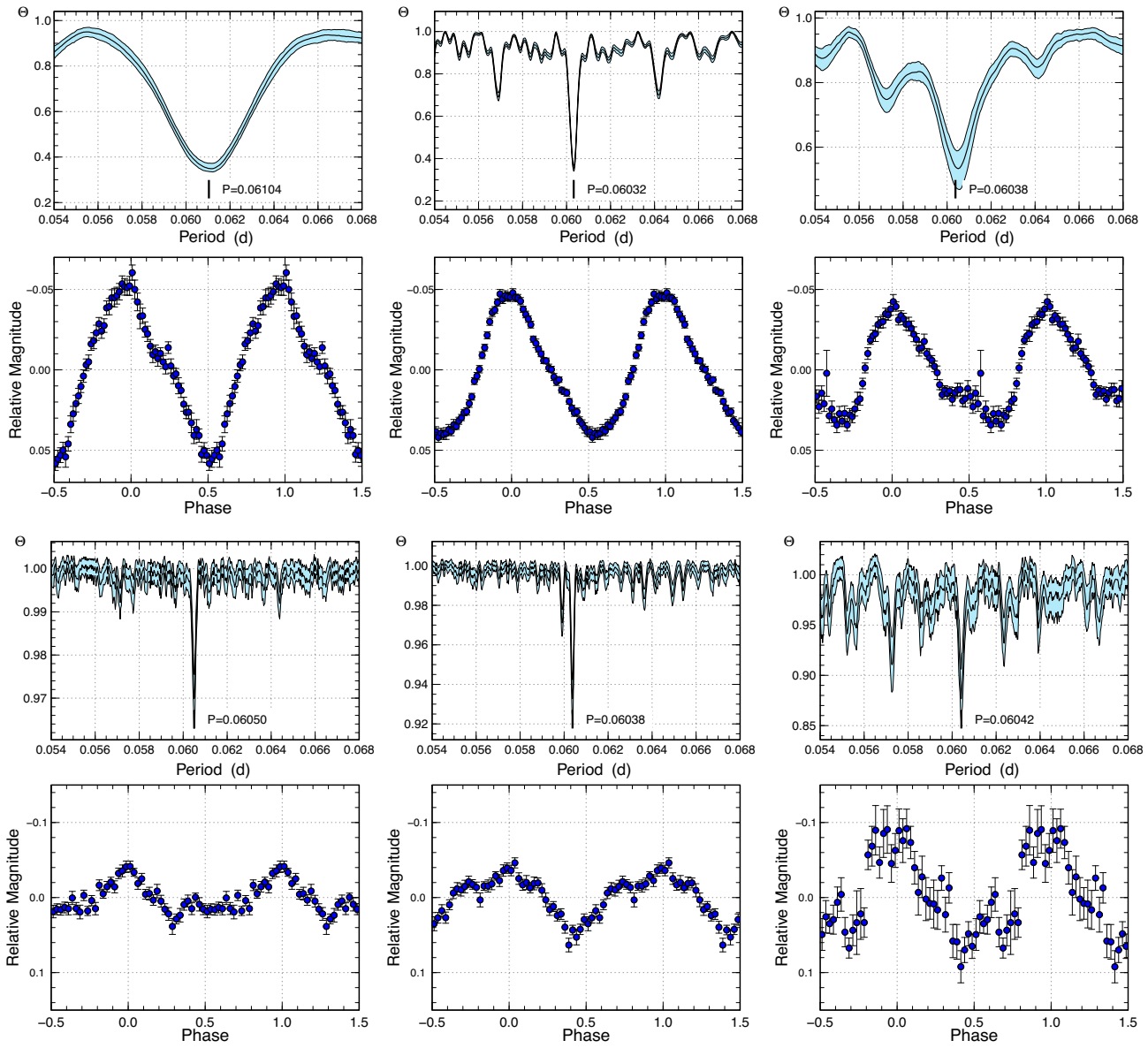

Fig. 3. Stage A superhumps, stage B superhumps, light modulations before stage A, stage La superhumps, stage Lb superhumps, and stage Lc superhumps in the 2018 superoutburst of EG Cnc. The upper panels are Θ-diagrams of our PDM analysis and the lower panels are phase-averaged profiles. Upper left: Stage A superhumps (BJD 2458399.7–2458400.8). Upper middle: Stage B superhumps (BJD 2458400.8–2458408.7). Upper right: Light modulations before stage A (BJD 2458398.4–2458399.7). Lower left: Stage La superhumps (BJD 2458412.9–2458431.7). Lower middle: Stage Lb superhumps (BJD 2458435.5–2458453.7). Lower right: Stage Lc superhumps (BJD 2458457.5–2458471.7). (Color online)

0.060383(7) d, and the derivative of the superhump period during stage B ($P_{\rm dot}$) is $4.8(5.6) \times 10^{-5}$ s s^{-1}.

3.3 Multi-wavelength behavior and color variations

We have explored the daily variation of optical and NIR colors during the rebrightening stage of the 2018 superoutburst in EG Cnc. In figure 5, we show daily averages of the colors and the V-band light curve. The $B - V$ and $J - K_{\rm s}$ colors are extracted from the data obtained by KU1 and HHO, respectively. During quiescence between rebrightenings, the averaged $B - I$ color was 0.8, which is redder than that in quiescence in typical DNe (Bailey 1980). This phenomenon is consistent with the unusually red $V - I$ color in the rebrightening phase of the previous superoutburst of this object (Patterson et al. 1998). Also, the $J - K_{\rm s}$ color became bluer. On the other hand, the $B - I$ color became bluer during each rebrightening.

Let us consider the continuum emission from a WZ Sge star. In WZ Sge stars, the radiation from the accretion disk is dominant over UV, optical, and NIR wavelengths, since

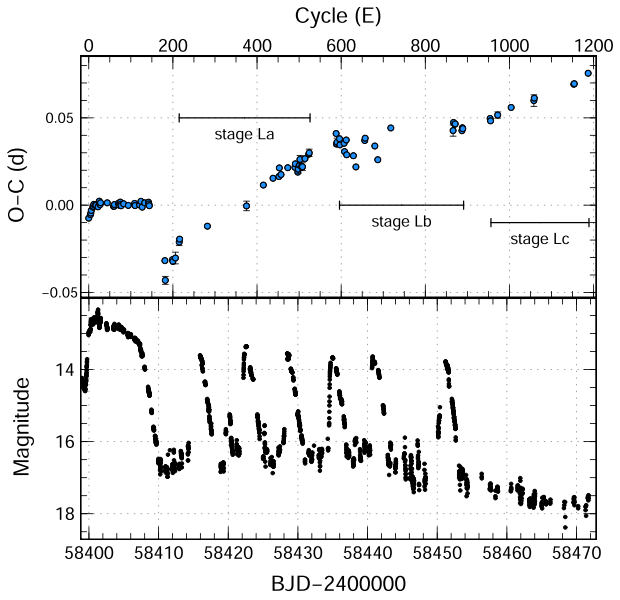

Fig. 4. $O - C$ curve of the times of superhump maxima and light curves during BJD 2458399.7–2458471.7. (Color online)

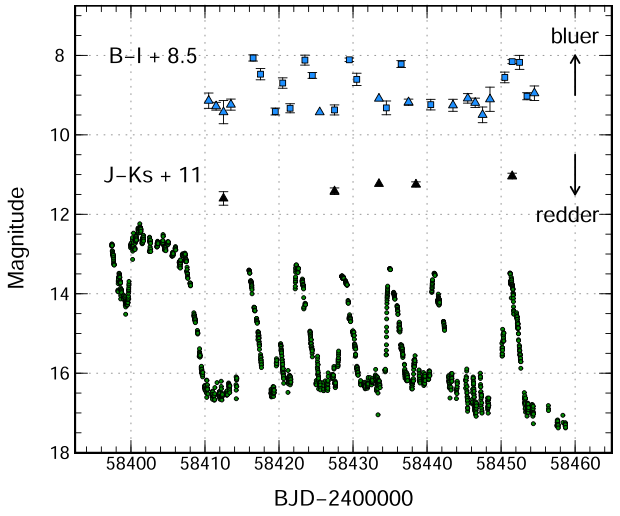

Fig. 5. Overall *V*-band light curve of the 2018 superoutburst of EG Cnc, and variations of $B - I$ and $J - K_s$ colors. The triangles and rectangles represent the color in quiescence between rebrightenings and that in each rebrightening, respectively. (Color online)

the white dwarf and the secondary star are tiny and since the boundary layer emits X-rays. If the disk is optically thick and geometrically thin, the emission from the disk surface is approximately blackbody radiation. Generally, the temperature of the inner part is high and that of the outer part is low in the accretion disk since the gravitational potential of the white dwarf becomes deeper inwards in the disk. Simply, each annulus in the disk has a different temperature and multi-temperature blackbody emission synthesizes the radiation from the disk. In fact, the observed continuum spectra of the disk around the outburst maximum agree well with multi-color blackbody emission expected from the standard-disk model (Shakura & Sunyaev 1973; Horne & Cook 1985). It is considered that UV photons come mainly from the inner part of the disk. A Rayleigh-Jeans slope of the multi-color blackbody typically exists around optical and NIR wavelengths in the spectrum, which depends on the disk radius and the temperature of the outermost part of the disk. The $B - I$ color is sensitive to the temperature distribution of the outer disk and the $J - K_s$ color is affected by the activity at the lower-temperature outermost region of the disk and the time variation of the disk radius. The $B - I$ color of 0.8 in our observations corresponds to the blackbody radiation of ∼7000 K. Also, the $J - K_s$ color of 0.2–0.6 corresponds to the blackbody radiation of ∼4000–7000 K.

According to the picture described above, the red $B - I$ and $J - K_s$ colors at the beginning of the rebrightening stage suggests the presence of the cool component at the outermost disk. If the low-temperature gas at the outermost disk is depleted with accretion during rebrightenings, i.e., the disk shrinks with time, the $J - K_s$ color in the quiescent state between rebrightenings should become bluer. The bluer $J - K_s$ color in our observations agrees with this idea. On the other hand, the bluer $B - I$ color during each rebrightening implies that the temperature of the outer disk increased at that time, because this region goes up to the outburst state. The $B - I$ color of 0.0 corresponds to the blackbody radiation of ∼18000 K, which is higher than the minimum temperature of the outburst state (see, e.g., Mineshige & Osaki 1983). For the solid confirmation, we need to analyze the spectral energy distribution of the disk, which is beyond the scope of this paper.

We have also investigated the color variation of the phase-averaged profile of stage B and late-stage superhumps. The phase-averaged profiles and the $V - R$ colors are exhibited in figure 6. The color became redder at the maximum of superhumps during stage B, while it became bluer after the main superoutburst.

Moreover, we have obtained multi-wavelength light curves during rebrightening by using the *Swift* satellite. The optical, UV, and X-ray light curves are exhibited in figure 7. This system was faint at X-ray wavelengths during the rebrightening stage, which suggests that the boundary layer between the inner disk rim and the white dwarf became optically thick during multiple rebrightenings because of the high accretion rate to the white dwarf (e.g., Pringle & Savonije 1979; Patterson & Raymond 1985). On the other hand, the UV light curve is sensitive to multiple rebrightenings and seems to well trace the optical one. The daily $U - B$ color is also displayed in the top panel of figure 7. Although the UV observations were performed using four different bands, we here treat them as the same *U* band for simplicity. The $U - B$ color became redder at least

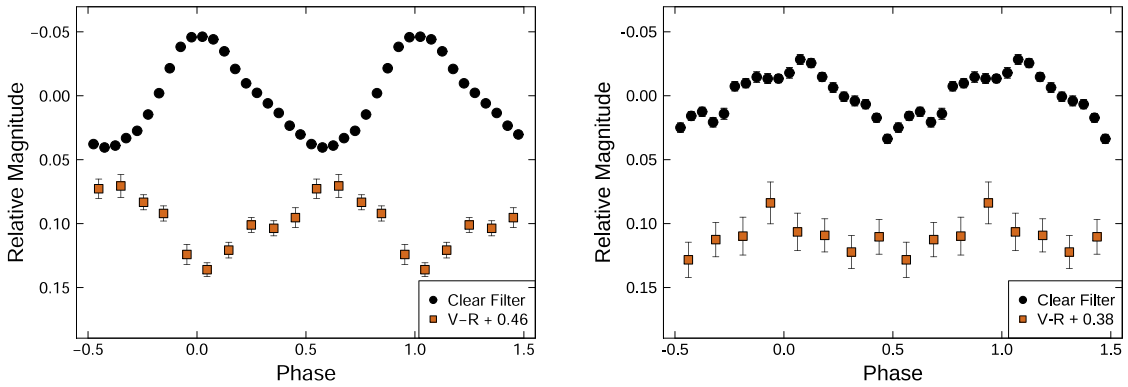

Fig. 6. Phase-averaged profile of superhumps and $V - R$ color. Left: Stage B superhumps (BJD 2458400.8–2458408.7). Right: Late-stage superhumps in quiescence between rebrightenings (BJD 2458412.9–2458471.7). (Color online)

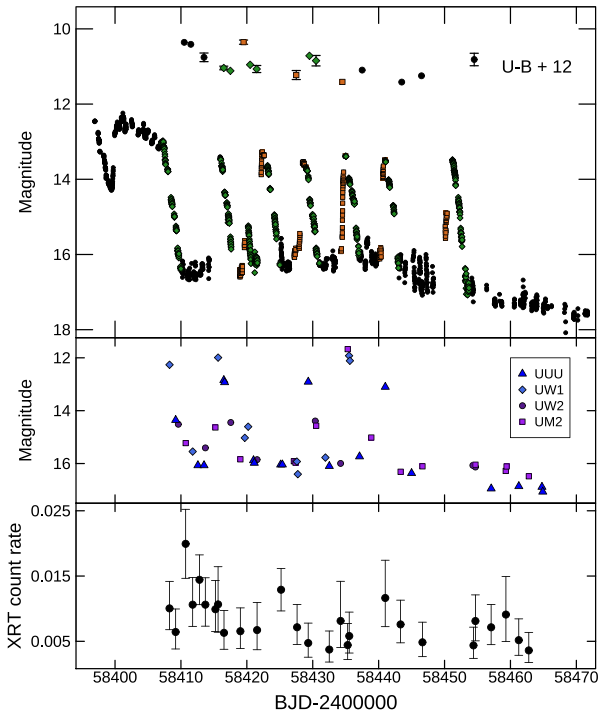

Fig. 7. Optical, UV, and X-ray light curves of the 2018 superoutburst of EG Cnc. In the top panel, we denote the fading and the rising parts as diamonds and rectangles, respectively. Also, we give the $U - B$ color in the top panel, which is denoted as different symbols corresponding to those of the light curve. (Color online)

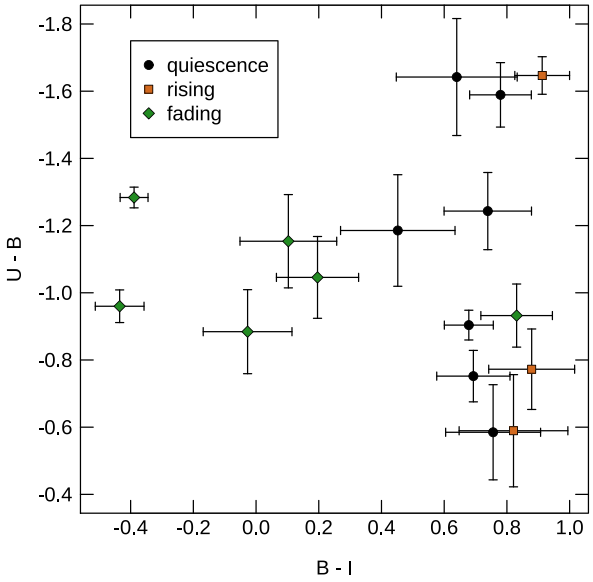

Fig. 8. Two-color plane composed of the $U - B$ and $B - I$ colors during the rebrightening phase. The circles, rectangles, and diamonds represent the data during quiescence between rebrightenings, the rising part, and the fading part, respectively. (Color online)

during quiescence between rebrightenings. As described in the second paragraph of this section, the inner part of the accretion disk is generally hotter than its outer part and UV photons are regarded as being released from the innermost region of the disk. The $U - B$ color is thus considered to be sensitive to the activity in the inner disk as expected by numerical simulations (Cannizzo & Kenyon 1987). The redder $U - B$ color during the rebrightening phase may represent that the inner region of the disk becomes cooler. The $U - B$ color seems to be at a similar level in comparison with the observed $U - B$ colors in other dwarf novae (Bailey 1980; Echevarria & Jones 1983; Shugarov et al. 2018).

We also show a diagram of the daily $U - B$ and $B - I$ colors during the rebrightening phase in figure 8. We separate the colors into three intervals: the quiescence between rebrightenings, the rising part, and the fading part. The $U - B$ color during the rising part and quiescence has a large dispersion, because that color became redder during the rebrightening phase as described above. Despite the large error bars, we see the trend that the $B - I$ colors are reddest at the rising part, and are bluest at the fading part. The $B - I$ color was slightly redder at the rising part of each rebrightening than that in quiescence and would represent the change in the temperature distribution of the outer disk and the disk radius. In the disk-instability model,

the disk rapidly expands at the onset of outbursts and the cool outer region temporarily expands before the outer disk edge completely goes up to the hot state (Ichikawa & Osaki 1992) and the color should become redder only at the very early stage of the outbursts. Our observations are consistent with this picture. On the other hand, the $B - I$ color around the light maximum and/or at the fading part became much bluer, although there is one exception observed at the small brightening between the first and the second rebrightenings. This behavior agrees with the interpretation that the outer disk became hotter during each rebrightening, as described in the third paragraph of this subsection. The small rebrighetening between the first and the second rebrightenings is likely to have been limited in the narrow region of the disk at that time. Then the temperature of the outer disk does not rise very much, which keeps the $B - I$ color red.

4 Discussion

4.1 Is EG Cnc one of the best candidates for period bouncers?

We firstly estimate the mass ratio of EG Cnc by using the stage A superhump period that we have derived (see subsection 3.2) and the orbital period [0.05997(9) d] reported by Patterson et al. (1998), complying with the method proposed by Kato and Osaki (2013). The superhump period is basically determined by the dynamical precession of the eccentric disk and the pressure effect decreasing the precession rate (Lubow 1992; Hirose & Osaki 1993), and hence, the apsidal precession rate of the eccentric disk, $\omega_{\rm pr}$, is approximately formulated as

$$\omega_{\rm pr} = \omega_{\rm dyn} + \omega_{\rm press}, \tag{1}$$

where $\omega_{\rm dyn}$ and $\omega_{\rm press}$ are the dynamical precession rate and the precession rate by the pressure effect, respectively. Stage A superhumps are the developing superhumps and are believed to represent the dynamical precession at the 3 : 1 resonance radius. According to Hirose and Osaki (1990), the dynamical precession rate is expressed as:

$$\omega_{\rm dyn}/\omega_{\rm orb} = Q(q)R(r), \tag{2}$$

where $Q(q)$ and $R(r)$ are the functions of the mass ratio and that of a given radius in the accretion disk, respectively [see equations (1) and (2) in Kato and Osaki (2013) for details], and r is expressed as $[3^2(1+q)]^{-1/3}a$, which is the 3 : 1 resonance radius in the case of stage A superhumps. Here a is the binary separation. By using equation (2), the mass ratio of EG Cnc is estimated to be 0.045(5) which is consistent with the $P_{\rm dot}$ value derived in subsection 3.2 and the type-B rebrightening (see also figure 17 in Kato 2015).

However, the period of stage A superhumps might be diluted by other light modulations before stage A (see subsection 3.2). For confirmation, we have constrained the mass ratio by using late-stage superhumps. The constant period of late-stage superhumps observed a long time after the main superoutburst would represent the dynamical precession at the outer rim of the disk as suggested by Kato and Osaki (2013). If we know the mass ratio, the disk radius can be estimated from equation (2). We thus can constrain the mass ratio by using the period of stage Lc superhumps, if we determine the range of the disk radius. According to Kato and Osaki (2013), the disk radius after the rebrightening phase in WZ Sge stars ranges between the Lubow–Shu radius (Lubow & Shu 1975) and the 3 : 1 resonance radius. The derived limit of the mass ratio of EG Cnc is 0.019–0.057 with 95% confidence intervals. We take the median value as 0.048 since the disk radius long after the superoutburst accompanied by type-B rebrightening is empirically 0.30–0.32a (Kato & Osaki 2013), which is consistent with the estimated mass ratio in the previous paragraph within 1σ errors.

Our results thus allow a larger mass ratio for EG Cnc in comparison with the estimates in Patterson et al. (1998) and Patterson (2011). The mass ratio of this object would be underestimated in the past since the period of stage B superhumps was used for the estimation, as pointed out by Nakata et al. (2013). The evolutionary stage of EG Cnc is exhibited in the q–$P_{\rm orb}$ plane as figure 9 based on our estimates of the mass ratio. This object still seems to be one of the good candidates for period bouncers, since the mass ratio and the orbital period are similar to those of other period-bouncer candidates (the diamonds in figure 9), even if we consider the wide range of the possible mass ratio.

Also, we have found some characteristic observational features which period-bouncer candidates share in the 2018 superoutburst of EG Cnc. The mean amplitude of superhumps in the main superoutburst was smaller than that of ordinary WZ Sge-type stars (more than 0.1 mag) (see also subsection 3.2). The fading rate of the middle of the plateau stage in which stage B superhumps were observed was small, 0.098 mag d^{-1}, which indicates a slow decline (see also Kimura et al. 2018). These properties are considered to originate from weak tidal dissipations due to extremely low-mass secondary stars. This idea was already described in detail by Kimura et al. (2018).

However, the recurrence time of superoutbursts and the duration of stage A superhumps in EG Cnc are shorter than those of the other candidates (see, e.g., Nakata et al. 2014; Kimura et al. 2018). Although the duration of stage A superhumps was possibly longer than that we presented in

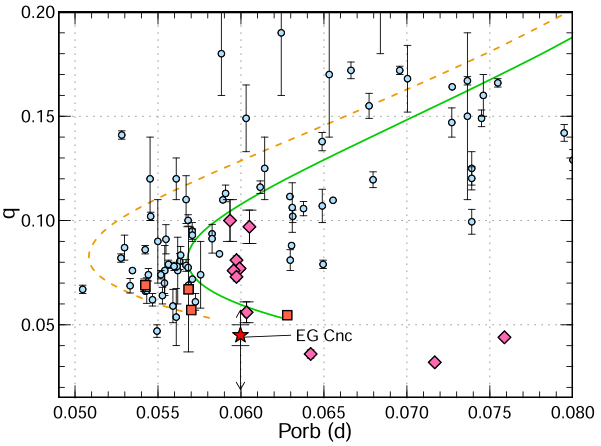

Fig. 9. $q - P_{\rm orb}$ relation of the candidates for period bouncers and ordinary WZ Sge-type DNe. The star, diamonds, rectangles, and circles represent EG Cnc, other candidates for period bouncers among the identified WZ Sge-type DNe, the candidates for period bouncers among eclipsing CVs, and ordinary WZ Sge-type DNe, respectively. The possible range of the mass ratio of EG Cnc is represented as the arrow underlying the star. The dashed and solid lines represent an evolutionary track of the standard scenario and that of the modified evolutionary theory, respectively, which are derived from Knigge et al. (2011). (Color online)

subsection 3.2, it is still less than a few days even if we consider the zero-point of the superhump amplitude expected from the time evolution of the amplitude given in the middle panel of figure 2. Since the long duration of stage A superhumps is considered to originate from the very small tidal effect caused by the low-mass star, and since the long recurrence time of superoutbursts would be due to the very low mass-transfer rate from the low-mass secondary, the short duration of stage A superhumps and the short recurrence time of superoutbursts in EG Cnc seem to be inconsistent with its low binary mass ratio. Although it is unclear where this inconsistency comes from, as for the short recurrence time, the sustained eccentricity in the disk expected from the long-lasting superhumps in this object might contribute, because the tidal dissipation of the disk by the secondary star increases the viscosity in the disk (Ichikawa & Osaki 1994). The temporal increase of the viscosity in the elliptical disk may be long-lasting even after superoutbursts, although the viscosity would gradually become lower with time.

4.2 Luminosity dip in the plateau stage

Kimura et al. (2016a) proposed that the slow development of the 3 : 1 resonance tidal instability cannot keep the efficient removal of the angular momentum from the outer disk after the fading of the 2 : 1 resonance due to weak tidal torques by the small secondary star in extremely low-q objects, which makes a luminosity dip in the middle of the plateau stage in the main superoutburst. However, the dip in the 2018 superoutburst in EG Cnc may be caused by a different reason, since the disk mass accumulated before that superoutburst seems to be small. EG Cnc entered one normal outburst between the 1996–1997 superoutburst and the 2018 superoutburst and some of the disk mass seems to have been depleted at that time. Although the disk is believed to expand far from the 2 : 1 resonance radius at the onset of superoutbursts in extremely low-q objects (period-bouncer candidates), there may be a possibility that the disk radius did not exceed the 2 : 1 resonance in the 2018 superoutburst of EG Cnc because of the small amount of mass stored in the disk.

We thus consider that the brightening before the dip in the 2018 outburst of EG Cnc is probably a precursor, i.e., a normal outburst triggering a superoutburst, which is usually observed before the superoutbursts in SU UMa-type stars (see, e.g., Osaki & Kato 2013), as confirmed in the 2015 superoutburst of AL Com, another WZ Sge star, which was triggered after only 1.5 yr quiescence (Kimura et al. 2016b).

4.3 Implications to the mechanism of rebrightenings

The light curve in the rebrightening stage of the 2018 superoutburst in EG Cnc was completely the same as that of its previous superoutburst in 1996–1997 despite the difference in the light curve of the main superoutburst (see figure 1). This is the second example following the 2015 superoutburst in AL Com (Kimura et al. 2016b). In the case of AL Com, the duration of the type-A (long duration) rebrightening was a little shorter in its 2015 superoutburst than that in its 2013 superoutburst (see also Kato et al. 2014b). However, not only the rebrightening type but also the timing of each rebrightening were the same between the two superoutbursts in EG Cnc. This phenomenon strengthens the interpretation proposed by Kimura et al. (2016b), that is, the rebrightening pattern is inherent to each object. The rebrightening type would be independent of the amount of the initial disk mass at the beginning of superoutbursts. This idea is consistent with the picture that the rebrightening type is related to the evolutionary stage of DNe, which was suggested by Kato (2015). Kato (2015) also noticed that WZ Sge showed the same type of rebrightening in its superoutbursts despite a little decrease in the duration of the plateau stage of the main superoutburst, and other WZ Sge-type DNe that entered superoutbursts more than twice exhibited the same type of rebrightening every superoutburst (Kato et al. 2009; Pavlenko et al. 2012; Kato et al. 2015). This agrees with the above interpretation.

The physical mechanism of rebrightenings observed in WZ Sge stars is unclear. As mentioned in the Introduction, two possibilities have been proposed as the trigger of rebrightening to date: the enhancement of the mass transfer by irradiation (Hameury 2000; Patterson et al. 2002) and the mass reservoir outside the 3 : 1 resonance radius (Kato et al. 1998; Hellier 2001). As for the multiple rebrightenings observed in EG Cnc, we have detected superhumps during the rebrightening phase of the 2018 outburst of EG Cnc, and the $B - I$ and $J - K_s$ colors were redder than those in the typical quiescence (see subsection 3.3). This may suggest that substantial mass was left at the outermost region in the disk, which supplies some materials to the inner disk, as many other optical and NIR observations suggested in the past (T. Kato et al. 1997;[1] Patterson et al. 1998; Uemura et al. 2008; Nakata et al. 2014; Isogai et al. 2015; Tampo et al. 2020). Also, the redder color of $B - I$ at the beginning of each rebrightening may indicate the disk expansion (see also figure 8). This contradicts the enhanced mass transfer hypothesis since in that scenario the influx of low specific angular momentum material from the secondary makes the disk shrink at the onset of outbursts, which is reproduced by numerical simulations (Ichikawa & Osaki 1992). The bluer $i - z$ and $J - K_s$ colors during the rebrightening phase may indicate the depletion of the mass reservoir by accretion. We thus have found positive evidence for the mass reservoir model, while we have not for the enhanced mass-transfer model.

If the disk possesses a lot of cool material even after the main superoutburst, the small increase of the viscosity could reproduce sustained rebrightenings as observed in EG Cnc, which was proposed by Osaki et al. (2001). We have confirmed that the optical flux in the quiescence between rebrightenings in the 2018 superoutburst of EG Cnc was higher than that in the quiescence before the main outburst and after the end of the rebrightening phase (see figure 1). Since more energy should be dissipated due to more efficient angular-momentum transfer, if the viscosity increases in the disk, the increase of the optical flux may represent the temporary enhancement of the viscosity of the disk. Osaki et al. (2001) considered that the temporary enhancement of the viscosity is caused by MHD turbulence. We also consider that the strong tidal dissipation lasting even after the main superoutburst could contribute to the enhancement, as mentioned in subsection 4.1.

Recent theoretical work by Meyer and Meyer-Hofmeister (2015) suggested that the enhancement of the viscosity halts the cooling-wave propagation over the whole disk at the decline from the plateau stage of the main superoutburst, and repetitive reflections of the heating and cooling waves in the disk could be the source of the multiple rebrightenings. The heating and cooling waves are the transition waves propagating over the disk. The former occurs when a region goes up to the hot state and the latter occurs when a region goes down to the cool state. They considered that the inner disk is permanently hot and that the entire disk easily jumps between the hot state and the cool state by the repetitive reflections.

However, we have found that the $U - B$ color became redder during the rebrightening phase in the case of 2018 superoutburst in EG Cnc (see the top panel of figure 7). This would mean that the inner disk became cooler during the rebrightening stage (see subsection 3.3). Also, the U-band light curve is similar to the optical light curve. These imply that the heating and cooling waves would go back and forth not only at the outermost disk but also at the inner disk at some point in the rebrightening phase. On the other hand, the $B - I$ color maintains a similar level during quiescence between multiple rebrightenings (see also figure 5). Also, the rapid rise of the rebrightenings except for the last one suggests that most of the rebrightenings were triggered at the outer disk, i.e., outside-in outbursts. If the heating wave propagates outwards from the inner disk, we should always observe a slow rise at the beginning of each rebrightening, i.e., inside-out outbursts [see, e.g., Mineshige and Osaki (1985) for the difference between outside-in and inside-out outbursts]. Taking into account our results, the inner portion of the disk is unlikely permanently hot in EG Cnc and the heating wave would be newly triggered at the beginning of each rebrightening at the outer disk rather than repetitive reflections.

4.4 Color variations of superhumps

We have investigated the time evolution of the color variation of superhumps in subsection 3.3. The redder color at the superhump maximum during stage B was also confirmed in the other two WZ Sge stars (Isogai et al. 2015; Neustroev et al. 2017), although the different types of color variations were found in V455 And (Matsui et al. 2009). Imada et al. (2018) showed the color variations of stage B superhumps change with time in the two WZ Sge stars HV Vir and OT J012059.6+325545, and interpreted that the time-varying pressure effect working on the precessing disk (Lubow 1992; Hirose & Osaki 1993) causes the variety. The difference in the color variation of superhumps among WZ Sge-type stars maybe because of the time variation of the pressure effect and/or the difference of the color bands used for the analyses. We have explored the $V - R$ color, while Matsui et al. (2009) investigated the $V - J$ color, and the data did not cover the entire period of the stage B superhumps. On the other hand, we have confirmed the bluer color around the superhump maximum in the

post-superoutburst stage. This trend was confirmed also in SSS J122221.7−311525 (Neustroev et al. 2017).

The color variation of superhumps seems to be weaker after the main superoutburst (see also figure 6). Superhumps are regarded as being produced by periodic tidal stressing working on the eccentric disk (Whitehurst 1988; Hirose & Osaki 1990; Lubow 1991a). The difference in the amplitude of the color variation is likely attributable to the difference in the size of the region in which the eccentricity works. The wider the region that the eccentricity propagates over, the larger the change in the temperature, geometry, and/or density of the disk during each cycle of superhumps would be. The superhump period is the synodic period between the period of the prograde precession of the disk and the orbital period (Whitehurst 1988; Hirose & Osaki 1990; Lubow 1991a), and the period change during stage B is believed to represent that the eccentricity propagates over the entire disk (Kato & Osaki 2013). On the other hand, the period variation during the rebrightening phase would be moderate in comparison with that during stage B, since the late-stage superhumps included two constant-period stages.

5 Summary

We have analyzed our multi-wavelength photometric data during the 2018 superoutburst of the WZ Sge-type DN EG Cnc to investigate whether EG Cnc is a possible candidate for period bouncers and the origin of its multiple rebrightenings. The main results are as follows.

- The rebrightenings in the 2018 superoutburst of EG Cnc almost completely reproduced those in its previous superoutburst in 1996–1997. EG Cnc is the second object following AL Com, in which this kind of phenomenon was confirmed. This phenomenon implies that some parameters inherent to each object are related to the rebrightening type in WZ Sge-type stars.
- The binary mass ratio of EG Cnc is estimated to be 0.045(5) and the possible range is estimated to be 0.019–0.057 by using the period of the stage A superhumps and the late-stage superhumps that we have detected. Also, the amplitude of superhumps in the main superoutburst and the fading rate at the plateau stage where stage B superhumps were observed was small, which is common in period-bouncer candidates among WZ Sge stars. Although the interval between superoutbursts and the duration of stage A superhumps are short in this object in comparison with other candidates, the increase of the viscosity in the disk, which might be caused by the long-lasting elliptical disk suggested by the sustained late-stage superhumps, could affect at least the short recurrence time of superoutbursts. Taking into account the estimated mass ratio and some observational features common in period-bouncer candidates, we consider that EG Cnc is a possible candidate for period bouncers.
- The $B - I$ and $J - K_s$ colors were unusually red at the beginning of the rebrightening phase, and gradually became bluer in quiescence between rebrightenings with time. This would mean that cool material existed at the outermost disk before multiple rebrightenings and was depleted during the rebrightening phase. The slightly redder $B - I$ color at the rising part of each rebrightening suggests the disk expansion. These results support the idea of the mass reservoir as the mechanism of rebrightenings rather than the enhancement of the mass-transfer rate.
- The UV light curve traced the optical light variations of multiple rebrightenings well and the $U - B$ color became redder during the rebrightening phase, which means that the inner disk became cooler. The thermal-viscous instability may have newly occurred at each rebrightening.

Acknowledgment

This work was financially supported by Grants-in-Aid for JSPS Fellows for young researchers (M. Kimura). M. Kimura acknowledges support by the Special Postdoctoral Researchers Program at RIKEN. We are thankful to many amateur observers for providing a lot of the data used in this research. This work is also supported by the Optical and Near-infrared Astronomy Inter-University Cooperation Program. M. Kimura is grateful to K. Takagi, I. Otsubo, Y. Yamazaki, and H. Kimura at Higashi-Hiroshima Observatory and Y. Uzawa at Saitama University for engaging in the observation of this star. The work of N. Katysheva and S. Shugarov was supported by the Program of Development of Lomonosov Moscow State University 'Leading Scientific Schools', project 'Physics of Stars, Relativistic Objects and Galaxies'. The work by S. Shugarov was supported by the Slovak Research and Development Agency under the contract No. APVV-15-0458 and by the Slovak Academy of Sciences grant VEGA No. 2/0008/17. The work by P. A. Dubovsky, I. Kudzej, and S. Shugarov was supported by the Slovak Research and Development Agency under the contract No. APVV-15-0458. We thank the anonymous referee for helpful comments.

Supplementary data

The following supplementary data is available at PASJ online.

Tables E1– E2.

References

Bailey, J. 1980, MNRAS, 190, 119
Cannizzo, J. K., & Kenyon, S. J. 1987, ApJ, 320, 319
Cleveland, W. S. 1979, J. Am. Statist. Assoc., 74, 829
Echevarria, J., & Jones, D. 1983, Rev. Mex. Astron. Astrof., 5, 301
Fernie, J. D. 1989, PASP, 101, 225
Hameury, J.-M. 2000, New Astron. Rev., 44, 15

Hellier, C. 2001, PASP, 113, 469
Hirose, M., & Osaki, Y. 1990, PASJ, 42, 135
Hirose, M., & Osaki, Y. 1993, PASJ, 45, 595
Horne, K., & Cook, M. C. 1985, MNRAS, 214, 307
Huruhata, M. 1983, IBVS, 2401
Ichikawa, S., & Osaki, Y. 1992, PASJ, 44, 15
Ichikawa, S., & Osaki, Y. 1994, PASJ, 46, 621
Imada, A., Isogai, K., Araki, T., Tanada, S., Yanagisawa, K., & Kawai, N. 2018, PASJ, 70, 2
Imada, A., Kubota, K., Kato, T., Nogami, D., Maehara, H., Nakajima, K., Uemura, M., & Ishioka, R. 2006, PASJ, 58, L23
Ishioka, R., et al. 2002, A&A, 381, L41
Isogai, M., Arai, A., Yonehara, A., Kawakita, H., Uemura, M., & Nogami, D. 2015, PASJ, 67, 7
Kato, T. 2002, PASJ, 54, L11
Kato, T. 2015, PASJ, 67, 108
Kato, T., et al. 2009, PASJ, 61, S395
Kato, T., et al. 2010, PASJ, 62, 1525
Kato, T., et al. 2014a, PASJ, 66, 30
Kato, T., et al. 2014b, PASJ, 66, 90
Kato, T., et al. 2015, PASJ, 67, 105
Kato, T., Maehara, H., & Monard, B. 2008, PASJ, 60, L23
Kato, T., Nogami, D., Baba, H., & Matsumoto, K. 1998, in ASP Conf. Ser., 137, Wild Stars in the Old West, ed. S. Howell et al. (San Francisco: ASP), 9
Kato, T., Nogami, D., Matsumoto, K., & Baba, H. 2004, PASJ, 56, S109
Kato, T., & Osaki, Y. 2013, PASJ, 65, 115
Kimura, M., et al. 2016a, PASJ, 68, 55
Kimura, M., et al. 2016b, PASJ, 68, L2
Kimura, M., et al. 2018, PASJ, 70, 47
Knigge, C., Baraffe, I., & Patterson, J. 2011, ApJ, 194, 28
Kolb, U. 1993, A&A, 271, 149
Littlefair, S. P., Dhillon, V. S., Marsh, T. R., Gänsicke, B. T., Southworth, J., Baraffe, I., Watson, C. A., & Copperwheat, C. 2008, MNRAS, 388, 1582
Lubow, S. H. 1991a, ApJ, 381, 259
Lubow, S. H. 1991b, ApJ, 381, 268
Lubow, S. H. 1992, ApJ, 401, 317
Lubow, S. H., & Shu, F. H. 1975, ApJ, 198, 383
Matsui, R., et al. 2009, PASJ, 61, 1081
Meyer, F., & Meyer-Hofmeister, E. 2015, PASJ, 67, 52
Mineshige, S., & Osaki, Y. 1983, PASJ, 35, 377
Mineshige, S., & Osaki, Y. 1985, PASJ, 37, 1
Nakata, C., et al. 2013, PASJ, 65, 117
Nakata, C., et al. 2014, PASJ, 66, 116
Neustroev, V. V., et al. 2017, MNRAS, 467, 597
Osaki, Y. 1989, PASJ, 41, 1005
Osaki, Y. 1996, PASP, 108, 39
Osaki, Y., & Kato, T. 2013, PASJ, 65, 50
Osaki, Y., & Meyer, F. 2002, A&A, 383, 574
Osaki, Y., & Meyer, F. 2003, A&A, 401, 325
Osaki, Y., & Meyer, F. 2004, A&A, 428, L17
Osaki, Y., Meyer, F., & Meyer-Hofmeister, E. 2001, A&A, 370, 488
Patterson, J. 2011, MNRAS, 411, 2695
Patterson, J., et al. 2005, PASP, 117, 1204
Patterson, J., et al. 1998, PASP, 110, 1290
Patterson, J., et al. 2002, PASP, 114, 721
Patterson, J., & Raymond, J. C. 1985, ApJ, 292, 535
Pavlenko, E., et al. 2012, Mem. Soc. Astron. Ital., 83, 520
Pringle, J. E., & Savonije, G. J. 1979, MNRAS, 187, 777
Shakura, N. I., & Sunyaev, R. A. 1973, A&A, 24, 337
Shugarov, S. Y., Katysheva, N. A., Chochol, D., Krushevska, V. N., & Vozyakova, O. V. 2018, Ap&SS, 363, 100
Stellingwerf, R. F. 1978, ApJ, 224, 953
Tampo, Y., et al. 2020, PASJ, 72, 49
Templeton, M. R. 2009, AAVSO Alert Notice, 407, 1
Uemura, M., et al. 2008, PASJ, 60, 227
Warner, B. 1995, Cataclysmic Variable Stars (Cambridge: Cambridge University Press)
Whitehurst, R. 1988, MNRAS, 232, 35